A New Switching Sequences of SVPWM for Six-Phase Induction Motor with Features of Reduced Switching Losses

Shaikh Mohammed Suhel, and Rakesh Maurya, *Member, IEEE*

***Abstract*— In this paper, new SVPWM switching sequences for six-phase asymmetrical induction motor drives are derived with the aim to reduce inverter's switching losses. Total three switching sequences are introduced in this paper. These sequences are derived such that the phases get continuously clamped when a current of the phases is around its peak magnitude and hence reduced switching losses are recorded. The comparative performances of these modulation techniques are studied with two existing switching sequences. Simulation, analytical and experimental results are presented. Based on these results, it is found that new switching sequences reduce switching losses effectively in dual three phase inverters.**

***Index Terms*— Six-phase asymmetrical induction motor, stator current distortion, SVPWM and switching loss.**

I. Introduction

THE advent of new power electronic converters have allowed machine phases to be considered as variable parameters. In these configurations, six phase asymmetrical induction motor (SPAIM), has two star connected windings displaced by 30º, is frequently utilized configuration due to its potential benefits in high power drives application [1]-[3].

In six-phase SVPWM technique, the switching sequences derived in various papers [4-8] are based on 12-sector PWM techniques that utilize four voltage vectors along with null vectors in each sampling duration. The switching patterns in these aforesaid techniques produce asymmetrical pole voltages in which more than two transitions occur in each sampling period. To resolve this, 24-sector based SVPWM techniques which utilize one medium-large and three large voltage vectors are proposed in [9]. The performance of 24-sector based SVPWM techniques, in comparison with 12-sector based PWM techniques, is found superior in terms of stator current distortion. Due to this, the 24 sector based PWM techniques introduced in [9] are the most widely accepted techniques for SPAIM [10], [11]. The 24-sector based synchronized SVPWM for low switching frequency operation is proposed in [12]. A vector classification technique applied to 24-sector based SVPWM technique is discussed in [13]. The techniques introduced in [12], [13] utilize five active voltage vectors in each sampling period.

In carrier-based PWM techniques, injection of double zero sequence is first time studied in [14]. In this research work, a comparative analysis of 12-sector based SVPWM technique along with double zero sequence injection is carried out. The double zero sequence injection method using harmonic distortion factor (HDF) as a performance parameter, is investigated in [15]. A detailed study of carrier-based PWM sequences using a space vector approach is presented in [16], [17]. The comparison of carrier based PWM techniques along with 24-sector based PWM technique is discussed in [17]. Additionally, three new switching sequences are introduced in this paper [17], with the aim to reduce current distortion. Investigation on harmonic injection technique, to achieve high performance is presented in [10]. The aim of this research work [10] is to reduce the stator current distortion in carrier-based approach such that it is comparable to the techniques presented in [9].

In SVPWM techniques, the switching sequences strongly influence the various performance parameters. The discontinuous sequences influences switching losses, current distortion and torque ripple [6], [9], [13], [18]; and power factor in case of switching loss [19]-[23]. The attempt is made in [23], to develop new discontinuous sequences based on the continuous sequences proposed in the [17] with aim to reduce stator current distortion. However, the switching losses recorded in these newly sequences are higher. In three-phase system, various studies have been reported regarding the impacts of PWM techniques on switching loss [19], [20], [22], [24]-[28]. Some effort has been made to develop dedicated switching sequences that can reduce switching losses in three-phase inverter [19], [22]. However, in six-phase system, PWM sequences specifically designed to reduce switching loss have never been reported. In view of this, the combinations of two discontinuous sequences that derived in [9], [23] are modified, in this paper, such that reduction of switching loss for machine load can be obtained. In this paper, three new sequences are derived and compared with two widely utilized existing switching sequences. The simulation, analytical and experimental results are presented for a various operating range of power factor and speed.

Manuscript received March 30, 2021; revised May 06, 2021; accepted June 08, 2021. date of publication June 25, 2021; date of current version June 18, 2021.

Shaikh Mohammed Suhel is with the Department of Electrical Engineering, R.N.G.Patel Institute of Technology Bardoli, Surat, India.(e-mail: suhelshaikh21@gmail.com)

Rakesh Maurya is with the Department of Electrical Engineering, Sardar Vallabhbhai National Institute of Technology, Surat, India.(e-mail: rmaurya@eed.svnit.ac.in)

(Corresponding Author: Rakesh Maurya)

Digital Object Identifier 10.30941/CESTEMS.2021.00013

II. SPACE VECTOR PWM FOR SIX-PHASE INVERTERS

The SPAIM fed by Dual Three-phase VSIs (D3VSIs) is shown in Fig. 1. Similar to three-phase case, the phase voltages can be obtained from the switching states of six-phase inverters. For example, phase voltage V_{a1} can be calculated using:

$$V_{a1} = \frac{V_{dc}}{3}\{2(S_{a1}) - 1(S_{b1} + S_{c1})\} \quad (1)$$

where S_{n1} (n=a, b, and c) represents the switching state ('1' or '0') for upper switches and V_{dc} represents the dc bus voltage. Since 64 individual switching combinations are possible, 64 voltage vectors can be utilized to SPAIM. For ease of analysis, these voltages are transformed by applying (2):

$$[T] = \frac{1}{\sqrt{3}} \cdot \begin{bmatrix} 1 & \cos 4\theta & \cos 8\theta & \cos\theta & \cos 5\theta & \cos 9\theta \\ 0 & \sin 4\theta & \sin 8\theta & \sin\theta & \sin 5\theta & \sin 9\theta \\ 1 & \cos 8\theta & \cos 4\theta & \cos 5\theta & \cos\theta & \cos 9\theta \\ 0 & \sin 8\theta & \sin 4\theta & \sin 5\theta & \sin\theta & \sin 9\theta \\ 1 & 1 & 1 & 0 & 0 & 0 \\ 0 & 0 & 0 & 1 & 1 & 1 \end{bmatrix} \quad (2)$$

where $\theta=\pi/6$. All 64 phase voltages can be represented in three different planes, namely d-q plane, x-y plane and 0_1-0_2 plane. With isolated neutrals winding projection of reference vector in 0_1-0_2 plane is inherently zero [4] and hence neglected. By selecting different switching states, the obtained phase voltages are mapped in d-q and x-y planes as shown in Fig. 2. In Fig. 2, voltage vectors are represented by a decimal number equivalent to a binary number of switching states (S_{c2}, S_{b2}, S_{a2}, S_{c1},S_{b1},S_{a1}).

In next step, minimum four voltage vectors are selected during a sampling interval for controlling reference voltage vector magnitude in d-q plane and concurrently maintaining zero magnitudes in other plane. The dwell times for selected vectors are calculated using following equation:

$$\begin{bmatrix} t_1 \\ t_2 \\ t_3 \\ t_4 \end{bmatrix} = \begin{bmatrix} V_{sd}^1 & V_{sd}^2 & V_{sd}^3 & V_{sd}^4 \\ V_{sq}^1 & V_{sq}^2 & V_{sq}^3 & V_{sq}^4 \\ V_{sx}^1 & V_{sx}^2 & V_{sx}^3 & V_{sx}^4 \\ V_{sy}^1 & V_{sy}^2 & V_{sy}^3 & V_{sy}^4 \end{bmatrix}^{-1} \begin{bmatrix} V_{sd}^* T_s \\ V_{sq}^* T_s \\ V_{sx}^* T_s \\ V_{sy}^* T_s \end{bmatrix}_g \cdot (3)$$

Where V_i^k is the projection of i^{th} voltage vectors on i-axis and t_i is the dwell times of that vector. The x-y plane components in (3), represents harmonics which are mapped on x-y plane and thus $V_{xs}^* = V_{ys}^* = 0$. Finally, dwell time for zero voltage vectors are obtained from:

$$t_0 = T_S - (t_1 + t_2 + t_3 + t_4) \quad (4)$$

The expression (3) and (4) is a generalized equation that can be utilized for calculation of dwell times for voltage vectors from Fig. 2 in required sectors. The selection of switching vectors mainly depends on choice of PWM techniques. In next section, SVPWM techniques derived in [9, 23] are modified to reduce switching losses of D3VSIs. As discussed in [23], the discontinuous sequence, also termed here as bus clamping sequence, derived from 6SVM1 and 6SVM3 provide better performance. Hence, they are selected as a benchmark for designing new PWM sequences in this paper.

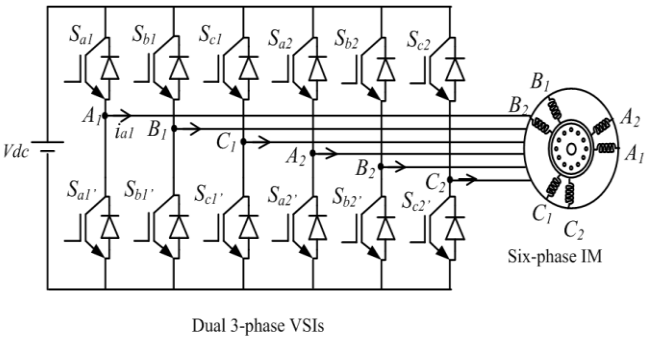

Fig. 1. Six-phase asymmetrical IM fed by dula 3-phase VSIs.

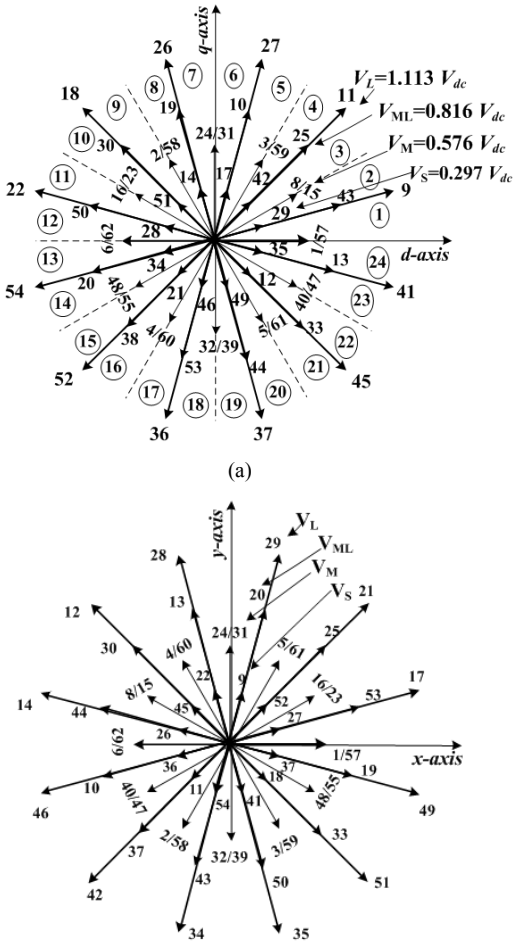

Fig. 2. Switching vectors on (a) d-q and (b) x-y plane.

III. SVPWM SWITCHING SEQUENCES

TABLE I presents the sequences utilized in first four sectors for 6SVM1 and 6SVM3 techniques. These sequences are derived and discussed in [9], [17], [23]. In TABLE I, S_n (where n=1 to 8) represents the sequence of four active vectors. TABLE II shows the continuous or discontinuous sequences develop by suitable placement of zero vectors (0, 63, 7, and 56) in the sequences of TABLE I.

The sector-wise switching sequences of first four sectors are only presented in TABLE II. In TABLE II, three newly developed sequences are presented with bold typeface. These newly designed sequences are derived such that the phases get

continuously clamped when a current of the phases is around its peak magnitude. The sequences 6SVM1-S1 and 6SVM3-S1 are derived from the sequences of 6SVM1-B2 and 6SVM3-B2. For example, the sequence 6SVM1-S1 is designed by adopting the sequences of 6SVM-B2 for odd numbers and 6SVM-B1 for even numbers of sectors as seen in TABLE II. Fig. 3 shows the modulating waves and switching pulses for PWM sequences. For digital implementation this modulating wave require certain modification [23]. However, to explain clamping duration the modulating wave without modification is withdrawn from DAC channel of the controller. As seen in TABLE II and Fig. 3 (a) and (b), the sequences 6SVM1-B2 and 6SVM2-B2 are not continuously clamped in phase a_1. In SPAIM, also in general for any lagging load, the phase current attains its peak after a half cycle duration over a fundamental period. For example, when SPAIM operates at 30° lagging power factor, phase a_1 attains its peak at the end of second sector (ωt =120°). It is beneficial, in terms of switching loss, if phase a_1 is clamped around these sectors. The newly developed sequences are designed based on this principle. As shown in Fig. 3 (c) and (d), 6SVM1-S1 and 6SVM3-S1 sequences clamp phase a_1 for positive rail of dc bus for three consecutive sectors, or in other words total 45° duration in a positive half cycle. In sequence 6SVM1-S1, only one phase is clamped during even number of sector while two phases are clamped during odd number of sectors as seen in TABLE II. In effect, total no. of switching during a sampling period is reduced to four or five in every odd or even sector respectively. Hence for maintaining switching frequency

TABLE I
6SVM1 AND 6SVM3 SVPWM SWITCHING PATTERNS

Switching Sequences of voltage vector			
S_1	41-9-11-15	S_5	40-41-9-11
S_2	57-41-9-11	S_6	41-9-11-3
S_3	9-11-27-59	S_7	1-9-11-27
S_4	8-9-11-27	S_8	9-11-27-31

TABLE II
SWITCHING PATTERNS AND PLACEMENT OF ZERO VECTOR

Sector:	1	2	3	4
	$90^\circ \le \omega t \le 105^\circ$		$120^\circ \le \omega t \le 135^\circ$	
6SVM1	56-S_1-7	56-S_2-7	0-S_3-63	0-S_4-63
Clamping Phases:	None	None	None	None
6SVM1-B1	56-S_1	S_2-7	0-S_3	S_4-63
Clamping Phases:	a_2	a_1	c_1	a_2
6SVM1-B2	S_1-7	56-S_2	S_3-63	0-S_4
Clamping Phases:	a_1,b_2	c_1,a_2	a_1,a_2	c_1,c_2
6SVM1-S1	**S_1-7**	**S_2-7**	**S_3-63**	**S_4-63**
Clamping Phases:	**a_1,b_2**	**a_1**	**a_1,a_2**	**a_2**
6SVM3	56-S_5-7	56-S_6-7	0-S_7-63	0-S_8-63
Clamping Phases:	None	None	None	None
6SVM3-B1	S_5-7	56-S_6	S_7-63	0-S_8
Clamping Phases:	b_2	c_1	a_1	c_2
6SVM3-B2	56-S_5	S_6-7	0-S_7	S_8-63
Clamping Phases:	c_1,a_2	a_1,b_2	c_1,c_2	a_1,a_2
6SVM3-S1	**S_5-7**	**S_6-7**	**S_7-63**	**S_8-63**
Clamping Phases:	**b_2**	**a_1,b_2**	**a_1**	**a_1,a_2**
6SVM1-3S	**S_1-7**	**S_6-7**	**S_3-63**	**S_8-63**
Clamping Phases:	**a_1,b_2**	**a_1,b_2**	**a_1,a_2**	**a_1,a_2**

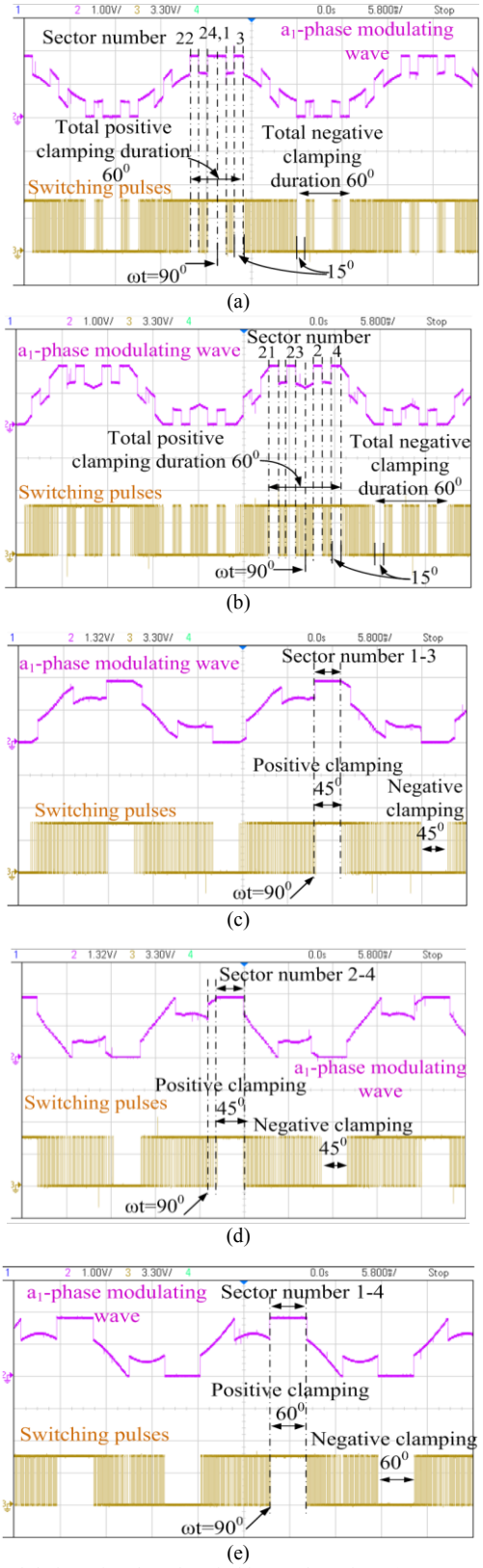

Fig. 3. Modulating signal and switching pulses for (a) 6SVM1-B2, (b) 6SVM3-B2, (c) 6SVM1-S1, (d) 6SVM3-S1, and (e) 6SVM1-3S.

same as in continuous sequence, the sampling frequency should raise by the rate of 12/9 ($1/kf$) for these two sequences. The increment of sampling frequency is higher (12/8) when two phases are clamped in every sector. As a result, HDF and

current distortion are reduced in this case. Considering this, one additional sequence 6SVM1-3S is derived and presented in last column of TABLE II. This PWM sequence is derived from the sequence of 6SVM1-S1 and 6SVM3-S1 and it is aimed to clamp two phases in every sector and phase-a_1 gets clamped for first four sectors. As a result, continuous clamping of phases, for 60° duration is obtained as shown in TABLE II and Fig. 3 (e). The coefficient factor *kf* is presented in TABLE III.

TABLE III
THE FACTOR *kf* FOR DIFFERENT SVPWM TECHNIQUES

SVPWM Techniques		*kf*	f_s
6SVM1	6SVM3	1	$f_s = \frac{1}{kf} f_{sw}$
6SVM1-B1	6SVM3-B1	5/6	
6SVM1-B2	6SVM3-B2	4/6	
6SVM1-S1	6SVM3-S1	9/12	
6SVM1-3S		4/6	

A. *Evaluation of Switching Loss in Various Sequences*

The analysis of switching losses is carried out in this section. Considering a_1 phase as a reference, in an inverter leg the switching loss mainly depends on stator current and number of switching transition during sub-cycle. In inverter leg a_1, the normalized switching loss can be calculated as [19]:

$$E_{a1} = \frac{n_{a1}|I_{a1}|}{I_m} = n_{a1}|\sin(\omega t - \phi)| \quad (5)$$

where i_{a1} is the fundamental phase current (rms), n_{a1} is the number of transition, I_m is maximum phase current and ϕ represents the angle of power factor. In (5), the sub-cycle duration for any PWM technique can be further normalized with respect to continuous PWM techniques for a given average switching frequency [19, 21, 28]:

$$P_{sub\_cycle} = \frac{n_{a1}|i_{a11}|}{I_m}\frac{f_s}{f_{SW}} = \frac{n_p|i_{p1}|}{I_m}\frac{1}{kf} \quad (6)$$

The variations of normalized switching losses are obtained by solving (6). The particular results obtain at unity power factor are presented in Fig. 4. In Fig. 4, the variation of energy loss for continuous SVPWM sequences is represented as a dotted line. As shown in Fig. 4 (a) and (b), the 6SVM1-B2 and 6SVM3-B2 clamp phase a_1 for 60° interval around the positive peak of fundamental voltage. During this interval no switching energy loss takes place. The energy that is lost on account of switching loss is the lowest in 6SVM1-B2 at unity power factor. This is due to zero switching when current of a_1-phase is around its peak. As the power factor angle goes on increasing switching loss also goes on increasing in this technique. For the lagging power factor load, this sequence is not a favorable option. The PWM sequences 6SVM1-S1 clamps phase a_1 between 90° to 135° and 6SVM3-S1 clamps phase a_1 between 105° to 150°. Consequently, during this interval the value of switching loss is zero as shown in Fig. 4 (c) and (d). At lagging power factor, around 0.866, the switching losses are reduced significantly in these two sequences than that of 6SVM1-B2 and 6SVM3-B2. When a 6SVM1-3S technique is selected, phase a_1 gets clamped to four consecutive sectors and as a result switching loss is zero for that duration as shown in Fig. 4 (e). At lagging power factor around 0.866, this sequence leads to the lowest switching loss.

The calculation for normalized per phase switching loss (avg.) in accordance with continuous SVPWM technique is as follows [22]:

$$P_{SW}(\phi) = 1/2 \int_{\phi}^{\pi+\phi} P_{sub\_cycle}(\theta,\phi)\, d\theta \quad (7)$$

The obtained results using (7) are plotted in Fig 5. When continuous techniques are utilized, the value of switching loss is unity as shown in 5. In discontinuous techniques, the switching losses are lower in comparison with continuous technique at a certain range of power factor angle. The switching loss in 6SVM1-3S is the lowest at high power factor in rated operating condition of the machine as shown in Fig. 5. At lagging power factor around 0.866, 6SVM1-3S leads to the lowest switching loss. When machine operated at no-load i.e., lower power factor condition, the 6SVM3-S1 reduces switching loss effectively.

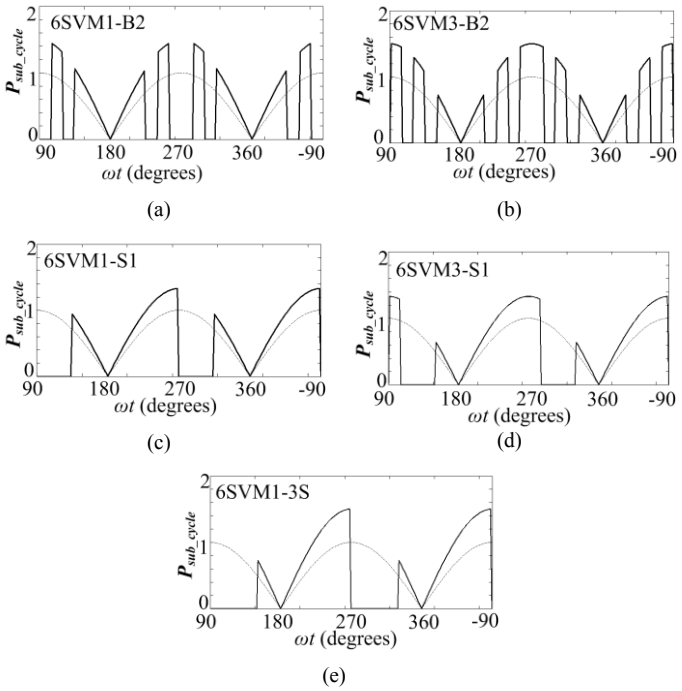

Fig. 4. Normalized switching losses of phase-a_1 during fundamental cycle and unity power factor.

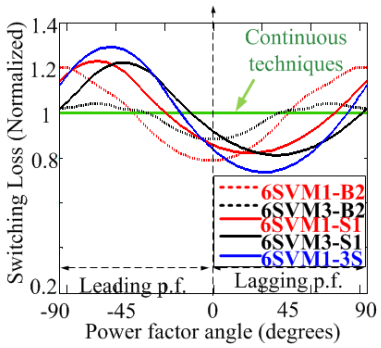

Fig. 5. Normalized switching losses in various SVPWM techniques.

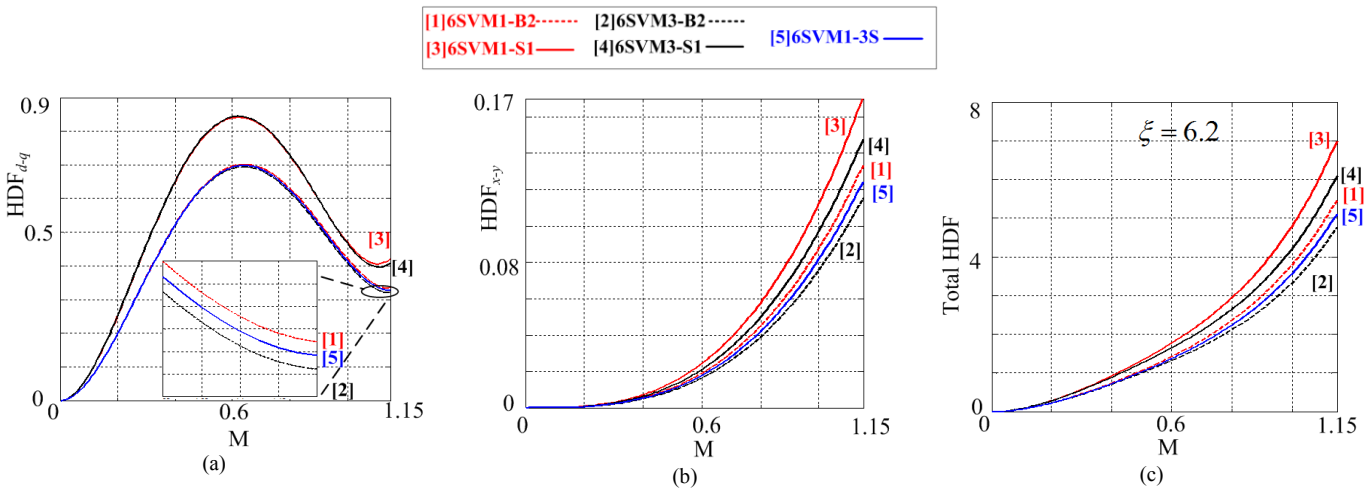

Fig. 6. HDFs in (a) d-q plane, (b) x-y plane and (c) Total HDFs for ξ=6.2.

B. *Evaluation of HDF in Various Sequences*

The additional effect of these newly developed discontinuous sequences is the difference in instantaneous error voltage vector leading to different harmonic characteristics. The steps for HDF evaluation of stator current ripple are discussed in [17], [23] in detail. So in this section, only the plots of HDFs are presented.

The results of HDFs for all SVPWM techniques are potted in Fig 6 (a) and (b). As discussed in [23], the HDF and current ripple of 6SVM1-B2 and 6SVM3-B2 techniques are lower than the other sequences. In the newly derived sequences, only placement of zero voltage vector is different than the 6SVM1-B2 and 6SM3-B2. For this reason, the curves of these PWM techniques are located closely. There is no significant difference observed in these techniques, as seen in previous comparative analysis of HDFs presented in [17, 23]. In these five techniques, two PWM techniques 6SVM1-S1 and 6SVM3-S1 result in slightly higher HDF as shown in these Fig. 6 (a) and (b). This is mainly due to the fact that lower sampling frequency is employed for these sequences in account of maintaining same average switching frequency. The 6SVM1-3S technique utilizes sequences of 6SVM1-B2 and 6SVM1-B3 alternatively and also in this case sampling frequency is higher than the 6SVM1-S1 and 6SVM3-S1. As a result, this technique provides marginally higher distortion than the 6SVM3-B2 and lower distortion than the 6SVM1-B2, as shown in Fig. 6 (a) and (b).

To evaluate total HDF from these two planes, the leakage coupling co-efficient ξ should be considered that define as the ratio of two inductances associated with these two planes [17]. For prototype machine used in experimentation, the value of ξ is 6.2. So, total HDFs for this value is also plotted as shown in Fig. 6 (c). Among all the discontinuous sequences, the 6SVM3-B2 produces the lowest distortion for various values of coefficient ξ as shown in Fig. 6 (c). In case of 6SVM1-3S, marginally higher distortion is observed in comparison with 6SVM3-B2. The other two newly developed sequences result in higher distortion among these five sequences.

IV. Analytical and Simulation Result

The simulation and analytical results are presented in this section. In all PWM techniques, switching frequency is maintained to 4.8 kHz while sampling frequency is calculated according to TABLE III. The dc link voltage of D3VSIs is kept to 280V. Fig. 7 (a) presents a comparison of the stator current THD in Simulink environment. As seen, stator current distortion in the 6SVM3-B2 is lower than the other PWM techniques. In case of 6SVM1-3S, the distortion is quite close or marginally higher than the 6SVM3-B2. The other two newly developed sequences result in the higher distortion due to lower sampling frequency. To validate further, the current distortion (analytial) is calculated uisng plots of HDF [23]:

$$THD\ (\%) = \frac{\frac{1}{\sqrt{6}}\left(\frac{V_{dc}T_s}{8}\right)\left(\frac{HDF_{d-q}}{L_\sigma^2} + \frac{HDF_{x-y}}{L_{lsxy}^2}\right)^{\frac{1}{2}}}{I_1} \times 100 \quad (8)$$

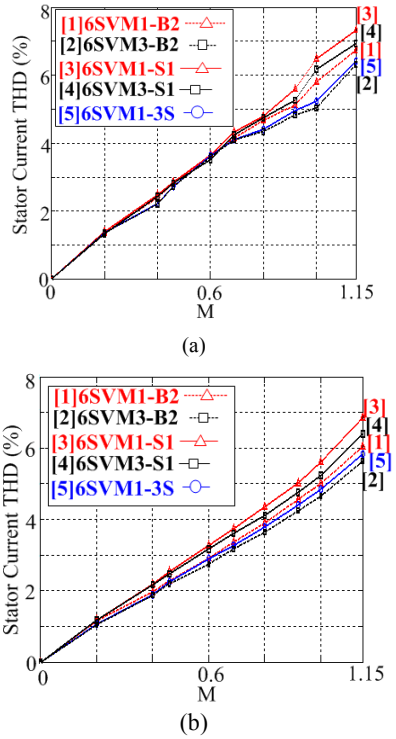

Fig. 7. Stator current THD: (a) analytical and (b) simulation.

where I_1 rpresents fundamental phase current (rms), L_σ and L_{lsxy} are the inductances associated with *d-q* and *x-y* planes. The calculated results of stator current harmonics are shown in Fig. 7 (b). Analytical results are obtained based on mathematical equation and exempted from all sorts of non-ideality. Both the results confirm the superiority of 6SVM3-B2 in terms of stator current distortion.

The D3VSIs model with parameters of IGBT and diodes are used in Simulink model to calculate the switching losses by means of lookup table. To obtain the switching loss at different power factor and maintaining the same magnitude of current, R-L network is used. The obtained values of switching losses don't differ with the use of R-L network instead of SPAIM in this case. Note that, for all simulations results presented here, mathematical model of SPAIM has been developed and utilized, except switching losses calculation.

Fig. 8 shows the obtained results of switching losses in various SVPWM sequences at different power factor angles. In Fig. 8, the obtained results are marked with the marker. In the same figure, the trajectories are obtained from Fig. 5 by multiplying all results with an obtained numerical value of switching losses in continuous PWM sequences. As seen, the evaluated switching losses agree well with relative values of analytical results. Clearly, the 6SVM1-3S significantly reduces switching losses in normal machine operating range. A significantly noticeable reduction around 24% at angle 30° is observed in comparison with standard 6SVM3-B2 technique. However, in 6SVM1-3S technique slightly higher stator current distortion (3 to 5%) is recorded in comparison with 6SVM3-B2.

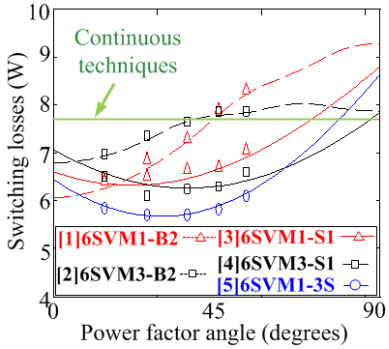

Fig. 8. Measured switching losses in various PWM techniques.

V. Experimental Results and Discussion

To validate the theoretical concept and simulation study, a prototype model of the six-phase asymmetrical machine rated with 1.5 kW, 200 V, 50 Hz, and 4-pole is designed. It has two three-phase stator windings groups with two isolated neutrals. The machine winding parameters are described in TABLE IV. The Semikron make inverter modules consist of three leg IGBT module SKM200GB12V, DC link capacitor and three-phase diode bridge rectifier. The IGBTs with anti-parallel body diodes are employed in this module which are rated with 1200 V and 200A. The inverters are controlled using STM32F407 controller board.

TABLE IV
Six Phase Induction Motor Parameters

Parameter	Value
Stator resistance (R_S)	4.35Ω
Rotor leakage inductance (L'_{lr})	0.02211H
Rotor resistance (R'_r)	4.61Ω
Magnetizing inductance (L_m)	0.430H
Stator leakage inductance in *d-q* plane (L_{lsdq})	0.01153H
Stator leakage inductance in *x-y* plane (L_{lsxy})	0.00525H
Mutual stator leakage inductance (L_{lm})	0.00314H
Leakage coupling coefficient (ξ)	6.2

Fig. 9. Test setup of SPAIM fed by D3VSIs.

TABLE V
Heat Sink Temperature Rise Due To Different SVPWM Techniques

SVPWM Techniques	(ΔT)° C (no-Load)	(ΔT)° C (2 Amp Load)
6SVM1-B2	6.8	10.4
6SVM3-B2	6.3	12.5
6SVM1-S1	5.8	10.9
6SVM3-S1	5.5	10.5
6SVM1-3S	5.2	9.8

To evaluate the switching loss of inverter, temperature rise in the heat sink is measured. The machine is running for 90 minutes for both condition (without loading and full load of 2 Amp) and increment in temperature over the ambient temperature is recorded. In experimentation, the modulation sequences are tested for 280V dc link, 4.8 kHz switching frequency and by maintaining modulation index to 1.15. TABLE V presents the results of measured temperature corresponding to different PWM techniques. As seen, temperature rise in 6SVM1-3S is less in comparison with other SVPWM sequences. Note that the switching and conduction loss both will contribute in temperature rise of D3VSIs.

Fig. 10 shows the recorded waveforms of stator current and corresponding harmonic spectra of PWM techniques. The stator current distortions are measured at different speed of drive by varying modulation index and plotted in Fig. 11.As mentioned earlier, all PWM sequences utilize the same active voltage vectors except one medium voltage vector during a sampling period. The dominant change in all the algorithms is

position of zero voltage vector. The placement of zero voltage vector in 6SVM1-S1 and 6SVM3-S1 leads to reduced sampling frequency. As a result, current distortion is higher in these two algorithms as shown in Fig 9 (c) and (d). As seen in figures, the waveforms quality and stator current THD of other three techniques are better than the 6SVM1-S1 and 6SVM3-S1. There is no significant difference in waveform quality in these three techniques. However, the 6SVM3-B2 leads to lower harmonic distortion among these techniques. As expected, the 6SVM1-3S results in marginally higher distortion than the 6SVM3-B2 and marginally lower distortion than the 6SVM1-B2 as shown in Fig. 10. These results are expected because in 6SVM1-3S switching sequences of 6SVM1-B2 and 6SVM3-B2 are used alternatively. These results validate the theoretical consideration.

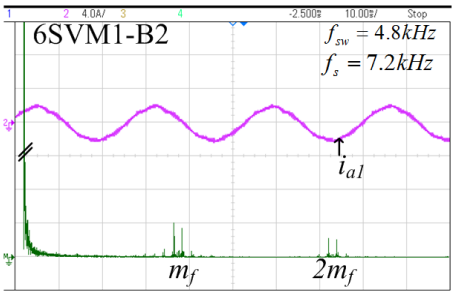

(a)

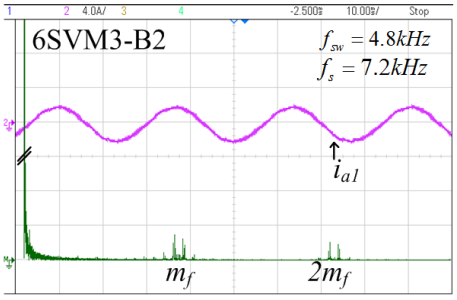

(b)

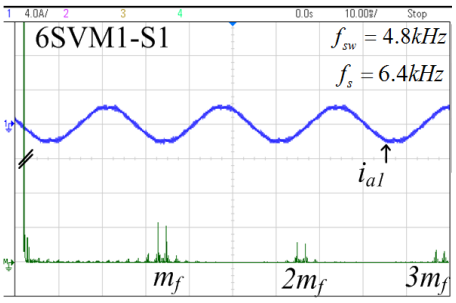

(c)

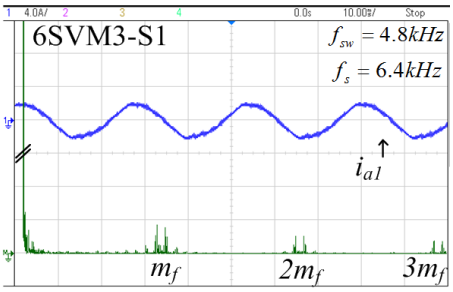

(d)

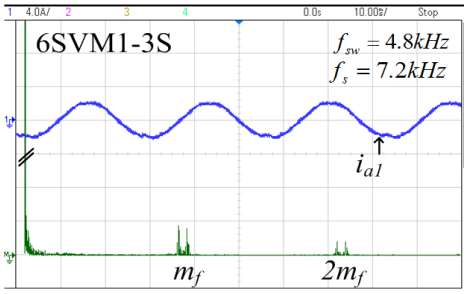

(e)

Fig. 10. Experimental result of stator current and FFT spectrum where scales of harmonic spectrum and current are 50 mA/division and 4.0 Amp/division respectively and frequency span is 20 kHz.

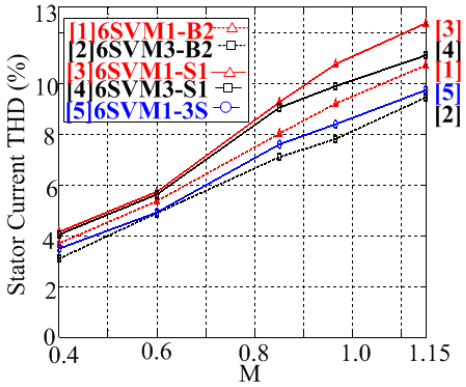

Fig. 11. Stator current distortion for various SVPWM sequences.

VI. Conclusion

In this study, three SVPWM techniques are developed and tested on a SPAIM. These SVPWM techniques are studied and compared with existing PWM sequences. The 6SVM1-3S technique provides excessive reduction in switching loss for the lagging power factor range when machine operates at rated condition of motor. However, this technique results in marginally higher current distortion in comparison with 6SVM3-B2. The technique 6SVM3-S1 results in the lowest switching loss at lower power factor range when machine operates at lightly loaded condition. The technique 6SVM3-B2 provides the lowest current distortion, but significantly higher switching losses are recorded than the 6SVM1-3S. The optimal choice is 6SVM1-3S at rated condition of machine with lagging power factor. In this condition, there is further chance to increase sampling frequency, higher than the 6SVM3-B2 and others, such that the switching losses are comparable with 6SVM3-B2. Certainly, with higher sampling frequency, the 6SVM1-3S provides the lowest current distortion. It is also found that, at lower power factor, the 6SVM3-S1 is a considerable option from the switching loss perspective.

References

[1] E. Levi, R. Bojoi, F. Profumo, H. Toliyat, and S. Williamson, "Multiphase induction motor drives-a technology status review," *IET Electric Power Applications,* vol. 1, no. 4, pp. 489-516, July 2007.

[2] E. Levi, "Recent Developments in High Performance VariableSpeed Multiphase Induction Motor Drives," *Sixth International Symposium Nikola Tesla Belgrade, Serbia.* , October, 2006.

[3] E. levi, "Multiphase electric machines for variable-speed applications," *IEEE Transactions on Industrial Electronics,* vol. 55, no. 5, pp.

1893-1909, May 2008.

[4] Y. Zhao and T. A. Lipo, "Space vector PWM control of dual three-phase induction machine using vector space decomposition," *IEEE Transactions on Industry Applications,* vol. 31, no. 5, pp. 1100-1109, Sep. 1995.

[5] D. Hadiouche, H. Razik, and A. Rezzoug, "Study and simulation of space vector PWM control of double-star induction motors," in *VII IEEE International Power Electronics Congress*, Mexico, 2000, pp. 42-47.

[6] D. Hadiouche, L. Baghli, and A. Rezzoug, "Space-vector PWM techniques for dual three-phase AC machine: analysis, performance evaluation, and DSP implementation," *IEEE Transactions on Industry Applications,* vol. 42, no. 4, pp. 1112-1122, 2006.

[7] A. Bakhshai, G. Joos, and H. Jin, "Space vector PWM control of a split-phase induction machine using the vector classification technique," in *Proc. IEEE Applied Power Electronics Conf. APEC*, Atlanta, GA, 1998, pp. 802-808.

[8] K. Marouani, L. Baghli, D. Hadiouche, A. Kheloui, and A. Rezzoug, "Discontinuous SVPWM techniques for double star induction motor drive control," in *IECON 2006-32nd Annual Conference on IEEE Industrial Electronics*, Paris, 2006, pp. 902-907.

[9] K. Marouani, L. Baghli, D. Hadiouche, A. Kheloui, and A. Rezzoug, "A new PWM strategy based on a 24-sector vector space decomposition for a six-phase VSI-fed dual stator induction motor," *IEEE Transactions on Industrial Electronics,* vol. 55, no. 5, pp. 1910-1920, 2008.

[10] P. Rakesh and G. Narayanan, "Investigation on Zero-Sequence Signal Injection for Improved Harmonic Performance in Split-Phase Induction Motor Drives," *IEEE Transactions on Industrial Electronics,* vol. 64, no. 4, pp. 2732-2741, April 2016.

[11] M. S. A. Shaikh and R. Maurya, "A Comparative Study of PWM Techniques for Multiphase Induction Motor Drives," *International Journal of Emerging Electric Power Systems,* vol. 19, no. 5, 2018.

[12] C. Wang, K. Wang, and X. You, "Research on Synchronized SVPWM Strategies Under Low Switching Frequency for Six-Phase VSI-Fed Asymmetrical Dual Stator Induction Machine," *IEEE Transactions on Industrial Electronics,* vol. 63, no. 11, pp. 6767-6776, 2016.

[13] W. Kun, Y. Xiaojie, W. Chenchen, and Z. Minglei, "An equivalent dual three-phase SVPWM realization of the modified 24-sector SVPWM strategy for asymmetrical dual stator induction machine," in *2016 IEEE Energy Conversion Congress and Exposition (ECCE)*, Milwaukee, WI, 2016, pp. 1-7.

[14] R. Bojoi, A. Tenconi, F. Profumo, G. Griva, and D. Martinello, "Complete analysis and comparative study of digital modulation techniques for dual three-phase AC motor drives," in *2002 IEEE 33rd Annual Power Electronics Specialists Conference, (pesc 02)*, Australia, 2002, pp. 851-857.

[15] J. Prieto, E. Levi, F. Barrero, and S. Toral, "Output current ripple analysis for asymmetrical six-phase drives using double zero-sequence injection PWM," in *IECON 2011-37th Annual Conference on IEEE Industrial Electronics Society*, Australia, 2011, pp. 3692-3697.

[16] P. R. Rakesh and G. Narayanan, "Analysis of sine-triangle and zero-sequence injection modulation schemes for split-phase induction motor drive," *IET Power Electronics,* vol. 9, no. 2, pp. 344-355, 2016.

[17] M. S. Shaikh and R. Maurya, "Realization of 24-Sector SVPWM with New Switching Pattern for Six-Phase Induction Motor Drive," *IEEE Transactions on Power Electronics,* vol. 34, no. 6, pp. 5079-5092, 2018.

[18] J. Prieto, M. Jones, F. Barrero, E. Levi, and S. Toral, "Comparative analysis of discontinuous and continuous PWM techniques in VSI-fed five-phase induction motor," *IEEE Transactions on Industrial Electronics,* vol. 58, no. 12, pp. 5324-5335, 2011.

[19] G. Narayanan, H. K. Krishnamurthy, D. Zhao, and R. Ayyanar, "Advanced bus-clamping PWM techniques based on space vector approach," *IEEE transactions on power electronics,* vol. 21, no. 4, pp. 974-984, 2006.

[20] J. W. Kolar, H. Ertl, and F. C. Zach, "Influence of the modulation method on the conduction and switching losses of a PWM converter system," *IEEE Transactions on Industry Applications,* vol. 27, no. 6, pp. 1063-1075, 1991.

[21] G. Narayanan, D. Zhao, H. K. Krishnamurthy, R. Ayyanar, and V. Ranganathan, "Space vector based hybrid PWM techniques for reduced current ripple," *IEEE Transactions on Industrial Electronics,* vol. 55, no. 4, pp. 1614-1627, 2008.

[22] D. Zhao, V. P. K. Hari, G. Narayanan, and R. Ayyanar, "Space-vector-based hybrid pulsewidth modulation techniques for reduced harmonic distortion and switching loss," *IEEE transactions on power electronics,* vol. 25, no. 3, pp. 760-774, 2010.

[23] R. Maurya and M. S. Shaikh, "Simplified implementation of SVPWM techniques for a Six-phase machine with reduced current distortion features," *IET Electric Power Applications,* pp. 1-1, 2019.

[24] A. M. Hava, R. J. Kerkman, and T. A. Lipo, "Simple analytical and graphical methods for carrier-based PWM-VSI drives," *IEEE transactions on power electronics,* vol. 14, no. 1, pp. 49-61, 1999.

[25] V. Blasko, "Analysis of a hybrid PWM based on modified space-vector and triangle-comparison methods," *IEEE Transactions on Industry Applications,* vol. 33, no. 3, pp. 756-764, 1997.

[26] R. O. Lyra, B. J. Cardoso Filho, V. John, and T. A. Lipo, "Coaxial current transformer for test and characterization of high-power semiconductor devices under hard and soft switching," *IEEE Transactions on Industry Applications,* vol. 36, no. 4, pp. 1181-1188, 2000.

[27] V. Kumar, S. Reddy, and G. Narayanan, "Measurement of IGBT switching characteristics and loss using coaxial current transformer," in *2012 IEEE 5th India International Conference on Power Electronics (IICPE)*, Delhi, India, 2012, pp. 1-6.

[28] S. M. Dabour, A. S. Abdel-Khalik, A. M. Massoud, and S. Ahmed, "Analysis of Scalar PWM Approach with Optimal Common-Mode Voltage Reduction Technique for Five-Phase Inverters," *IEEE Journal of Emerging and Selected Topics in Power Electronics,* pp. 1-1, 2018.

Shaikh Mo. Suhel received the B.E. degree in electrical engineering from Veer Narmad South Gujarat University, Surat, India, in 2006, and the M.Tech. degree with specialization in industrial electronics and the Ph.D. degree in electrical engineering from the Sardar Vallabhbhai National Institute of Technology, Surat, India, in 2010 and 2020, respectively. He is currently an Assistant Professor with the Department of Electrical Engineering, R.N.G.Patel Institute of Technology Bardoli, Surat, India. His research interests include multiphase induction motor and power electronics converter for drives application, and high power factor based dc-dc converter.

Rakesh Maurya (Member, IEEE) received the B.Tech. degree in Electrical Engineering from the Kamla Nehru Institute of Technology, Sultanpur, India, in 1998, and the M.Tech. degree in power electronics and electric drive and the Ph.D. degree in electrical engineering from the Indian Institute of Technology Roorkee, Roorkee, India, in 2002 2014, respectively. He is currently an Associate Professor with the Department of Electrical Engineering, Sardar Vallabhbhai National Institute of Technology, Surat, India. His current research interests include design of switching power converters, high power factor ac-dc converters, hybrid output converters, improved power quality converters for battery charging applications, power quality problems, advanced electric drives, and applications of real-time simulator for the control of power converters.